

AIAA PAPER
No. 75-1124

OPTIMUM FLIGHT PROFILES FOR SHORT HAUL MISSIONS

by
HEINZ ERZBERGER, JOHN F. BARMAN,
and
JOHN D. McLEAN
NASA Ames Research Center
Moffett Field, California

**AIAA Guidance and Control
Conference**

BOSTON, MASSACHUSETTS/AUGUST 20-22, 1975

For permission to copy or republish, contact the American Institute of Aeronautics and Astronautics,
1290 Avenue of the Americas, New York, N.Y. 10019.

OPTIMUM FLIGHT PROFILES FOR SHORT HAUL MISSIONS

Heinz Erzberger, John F. Barman,* and John D. McLean
Ames Research Center, NASA, Moffett Field, Calif. 94035

Abstract

An algorithm, based on the energy-state method, is derived for calculating optimum trajectories with a range constraint. The basis of the algorithm is the assumption that optimum trajectories consist of, at most, three segments: an increasing energy segment (climb); a constant energy segment (cruise); and a decreasing energy segment (descent). This assumption allows energy to be used as the independent variable in the increasing and decreasing energy segments, thereby eliminating the integration of a separate adjoint differential equation and simplifying the calculus of variations problem to one requiring only point-wise extremization of algebraic functions. The algorithm is used to compute minimum fuel, minimum time, and minimum direct-operating-cost trajectories, with range as a parameter, for an in-service CTOL aircraft and for an advanced STOL aircraft. For the CTOL aircraft and the minimum-fuel performance function, the optimum controls, consisting of airspeed and engine power setting, are continuous functions of the energy in both climb and descent as well as near the maximum or cruise energy. This is also true for the STOL aircraft except in the descent where at one energy level a nearly constant energy dive segment occurs, yielding a discontinuity in the airspeed at that energy. The reason for this segment appears to be the relatively high fuel flow at idle power of the engines used by this STOL aircraft. Use of a simplified trajectory which eliminates the dive increases the fuel consumption of the total descent trajectory by about 10 percent and the time to fly the descent by about 19 percent compared to the optimum.

Symbols

C = direct operating cost (DOC), dollars/trip
C₀ = constant cost component of DOC, dollars
C₁ = fuel-independent component of DOC, dollars
C_D = drag coefficient
C_{D0} = zero-lift drag coefficient
C_F = unit cost of fuel, cents/kg
C_L = lift coefficient
C_T = cost per unit flight time, dollars/hr
D(L,h,V) = drag, N
E = total energy, m
Ė = energy rate, m/sec
F = fuel consumed, kg
f_T = normalized thrust force function, N
f_F = normalized fuel flow function, kg/hr
g = acceleration of gravity, m/sec²
h = altitude, km
I = integrand
J = integral performance index
K(M) = induced drag factor
k₀ = lift curve intercept
k = slope of the lift curve
L = lift, N
M = Mach number
P = integrand performance index
p = atmospheric pressure, N/m²

p₀ = standard sea level atmospheric pressure, N/m²
R = range, km
R_{dn} = total descent range, km
R_{up} = total climb range, km
R_{ndn} = fraction of descent range
R_{nup} = fraction of climb range
S = wing reference area, m²
q = dynamic pressure, N/m²
T = total time of travel, min; temperature, °K
T_F = thrust force, N
t = time, min
V = airspeed, m/sec
W = mass, kg
W_F = fuel flow, tonnes/hr
α = angle of attack, deg
γ = path angle, deg; air specific heat ratio
ΔE = energy increment, m
Δt = time increment, min
Δ(M,C_L) = Mach number and lift coefficient correction to drag coefficient
δ = incremental variation or pressure factor
θ = temperature factor
λ = cruise efficiency, kg/km
λ* = minimum value of the cruise efficiency, kg/km
H = actual power setting, kilo rpm
ρ = air density, kg/m³
σ = fuel tradeoff coefficient
τ = atmospheric temperature, °K
τ₀ = standard sea level atmospheric temperature, °K

Subscripts

c = cruise, corrected, or climb
dn = descent
f = final
i = initial
in = inlet
max = maximum
min = minimum
opt = optimum
up = climb

Superscripts

(·) = time derivative
(⁻) = limiting value from below

Introduction

Sharply escalating fuel prices and the threat of future fuel shortages have generated strong interest in finding methods of reducing aviation fuel consumption that do not seriously affect the level of airline service. One such method, flight-path optimization, has the potential for saving significant quantities of fuel. Although there is a long history of flight-path optimization studies for all types of aircraft, modern approaches based on the variational calculus have been applied more frequently to supersonic military rather than subsonic civil aircraft missions.

*NRC Research Associate at Ames Research Center.

Subsonic aircraft missions can be roughly divided into long haul and short haul. In long-haul missions, which are characterized by long periods of cruise flight, the central problem in flight planning is optimizing the ground track and the altitude profile during cruise so as to use wind, temperature, and other atmospheric conditions to the greatest advantage. For flying the climbout and descent segments, long-haul operators use procedures supplied by the aircraft manufacturers. Such procedures are generally not optimum, in that they do not minimize a performance index such as time or fuel used and, because they affect only a small portion of the total flight path, they have a limited impact on long-haul flight performance.

These priorities are essentially reversed in short-haul missions (800 km or less). For these missions, the cruise segment is relatively short and therefore the climbout and descent segments play the dominant role in flight-path optimization. Moreover, the short range of these missions can yield a high degree of interdependence of the climbout, descent, and cruise optimization problems, suggesting that range should enter explicitly as a boundary value.

This paper describes a conceptually and computationally simple algorithm for calculating optimum flight paths with a range constraint. The algorithm is applied to flight profile optimization of two types of short-haul aircraft: a currently in-service CTOL jet and a future-design jet STOL aircraft (an augmentor wing with a supercritical airfoil). Minimum fuel and time-flight paths are computed for each aircraft. Furthermore, assuming that the relative costs of time and fuel are known, a procedure is given for selecting minimum direct-operating-cost (DOC) flight paths.

Definition of Performance Index

For a fixed aircraft configuration and a specified origin and destination, the primary factor that influences aircraft performance is operating procedure. For an airline, the performance goal is generally minimization of the direct operating cost (DOC) which consists of fuel cost, crew cost, maintenance cost, depreciation, and insurance. It is therefore of interest to determine a relationship specifying the dependence of DOC on flying time and fuel consumed. Relating DOC to fuel consumed is straightforward, but relating the other components of DOC to flying time is more difficult. A reasonable approach for the purpose of developing optimum flight procedures is to parameterize the cost of the DOC components, other than fuel, by the relation

$$C_1 = C_0 + C_T T \quad (1)$$

where C_0 is a cost component which is independent of time over the time scale of the mission, C_T is the cost per unit flight time, and T is the total flight time. Thus, the factor C_T should reflect the monetary value of flight time, exclusive of fuel cost. The total cost of the flight can therefore be written as

$$C = C_0 + C_T T + C_F \quad (2)$$

or in integral form as

$$C = \int_0^T (C_T + C_F) dt + C_0 \quad (3)$$

where C_F is the unit cost of fuel and W is the fuel flow rate. Since minimization of Eq. (3) depends only on the ratio C_F/C_T and not on C_0 , an equivalent performance index, which is more convenient for performance optimization, is

$$J = \int_0^T [\sigma W_F + (1-\sigma)] dt; \quad 0 < \sigma < 1 \quad (4)$$

where

$$\sigma = \frac{C_F/C_T}{1 + (C_F/C_T)} \quad (5)$$

The two extreme values of σ give the two important special cases of minimum time ($\sigma = 0$) and minimum fuel ($\sigma = 1$) performance indices.

Derivation of Optimization Algorithm

The approach to flight-path optimization taken here follows the trend in the recent literature of using the energy state formulation as the basis for computing the optimum flight paths.^{2,3} The rate of change of energy along the flight path is given by

$$\frac{dE}{dt} = [T_P(N, h, V) - D(N, h, V)] \frac{V}{W} \quad (6)$$

where

$$h = E - \frac{1}{2g} V^2$$

and T_P is the thrust, D the drag, L the lift, W the weight of the aircraft, h the altitude, V the airspeed, and g the acceleration of gravity. The controls which determine the flight path are taken as the power setting, N , and airspeed V . In accordance with the energy-state method, it will be assumed that lift is equal to weight in computing the drag. The flight path is also constrained to cover a specified range, R , which makes it necessary to introduce an additional state equation:

$$\frac{dR}{dt} = V \quad (7)$$

In Eq. (7) it is assumed that, except at isolated time instants, the flight-path angle, γ , is small - allowing the small-angle approximation, $\cos \gamma \approx 1$, to be made - and that the wind speed relative to the airspeed is negligible. The latter assumption is not necessary for the development that follows, but the effect of winds on the optimum flight path is not considered in this paper. Finally, the energy and range are specified at the beginning and end of the flight path:

$$\left. \begin{aligned} E = E_i \text{ and } R = R_i \text{ at } t = 0 \\ E = E_f \text{ and } R = R_f \text{ at } t = T \end{aligned} \right\} \quad (8)$$

Minimization of Eq. (4) subject to the constraints of Eqs. (6) and (7) and the boundary conditions of Eq. (8) is a frequently studied problem in optimum control. However, solutions published in the literature apply mostly to military supersonic aircraft missions. The most recent results in the field have generalized the energy-state method to include flight with turns, again for military aircraft applications. References 2, 3, and 4 provide a brief list of recent papers on this subject.

Application of the maximum principle results in a fourth-order, two-point boundary value problem consisting of the two state equations (6) and (7), the associated adjoint equations, and the boundary conditions (8). Numerical solution of two-point

boundary value problems of this type has proven to be difficult. Zagalski⁴ described a procedure for simplifying the two-point boundary value problem in the energy-state formulation. In this paper, an assumption about the structure of the optimum flight paths is similarly used to eliminate the need for the adjoint equation. The assumption is as follows:

Optimum flight paths for the problem defined here consist of three segments at most; in the first, energy increases monotonically, in the second it is constant along with the velocity, and in the third it decreases monotonically with time. The resulting flight paths may not be optimum for the problem as originally stated but should be very nearly so for most problems of interest.

To show how the assumption simplifies the computation of optimum flight paths, Eq. (4) is written as the sum of costs of the three segments:

$$J = \int_0^{T_{up}} (P)_{\dot{E}>0} dt + (P)_{\dot{E}=0} (T_{dn} - T_{up}) + \int_{T_{dn}}^T (P)_{\dot{E}<0} dt \quad (9)$$

where $P = \sigma W_T + (1-\sigma)$, T_{up} is the time at the end of the increasing energy segment, and T_{dn} is the time at start of the decreasing energy segment. The rate of change of energy, \dot{E} , is given by Eq. (6). Since airspeed is constant in cruise, the middle term corresponding to the cruise cost can be expressed as follows:

$$(P)_{\dot{E}=0} (T_{dn} - T_{up}) = \lambda R_c \quad (10)$$

In Eq. (10), R_c is the distance spent in cruise and λ , defined as the cruise efficiency, is evaluated at the cruise energy using the relationship

$$\lambda = \left(\frac{P}{V_c} \right)_{\dot{E}=0} \quad (11)$$

where V_c is the cruise airspeed. The cruise distance R_c is given by

$$R_c = R - R_{up} - R_{dn} \quad (12)$$

where

$$R_{up} = \int_0^{T_{up}} V dt, \quad R_{dn} = \int_{T_{dn}}^T V dt \quad (13)$$

and R_c must satisfy the inequality $R_c \geq 0$. Since by the assumption of the preceding paragraph, energy changes monotonically in the first and last terms of Eq. (9), energy can replace time as the independent variable in Eqs. (9) and (13). After applying the transformation $dt = dE/\dot{E}$ to these equations and substituting the appropriate integration limits, they become

$$J = \int_{E_i}^{E_{max}} \left(\frac{P}{\dot{E}} \right)_{\dot{E}>0} dE + \lambda R_c + \int_{E_f}^{E_{max}} \left(\frac{P}{|\dot{E}|} \right)_{\dot{E}<0} dE \quad (14)$$

$$R_{up} = \int_{E_i}^{E_{max}} \left(\frac{V}{\dot{E}} \right)_{\dot{E}>0} dE, \quad R_{dn} = \int_{E_f}^{E_{max}} \left(\frac{V}{|\dot{E}|} \right)_{\dot{E}<0} dE \quad (15)$$

Here, E_{max} refers to the maximum energy (cruise takes place at E_{max}). Note from Eq. (14) that since $R_c > 0$, the cruise efficiency λ should be chosen as small as possible in the process of minimizing J described below. Equations (12), (14), and (15) can be combined into a single equation:

$$J = \int_{E_i}^{E_{max}} \frac{(P-\lambda V)}{(\dot{E})_{\dot{E}>0}} dE + \int_{E_f}^{E_{max}} \frac{(P-\lambda V)}{|\dot{E}|_{\dot{E}<0}} dE + \lambda R \quad (16)$$

If we assume for the moment that E_{max} is known, then Eq. (16) can be minimized by performing three independent algebraic minimizations. The first optimizes cruise conditions and consists of minimizing λ at E_{max} as noted above. The remaining two problems are the minimization of the two integral cost terms in equation (16). They are minimized by choosing power settings and airspeeds as functions of E so that each of the two integrands is minimized at all values of the independent variable E throughout its integration interval. The minimization of each integrand must obey different constraints on the controls, namely, η and V must be such that $\dot{E} > 0$ for the increasing energy segment and $\dot{E} < 0$ for the decreasing one. In addition there are constraints on the power setting and airspeed which depend on the energy. These minimizations, defined below, ensure that J is minimum for each choice of E_{max} .

$$\lambda_{opt}(E_{max}) = \min_{\eta, V} \left(\frac{P}{V} \right)_{\dot{E}=0} \quad (17)$$

$$I_{up}(E, E_{max}) = \min_{\eta, V} \left(\frac{P - \lambda_{opt} V}{\dot{E}} \right)_{\dot{E}>0} \quad (18)$$

E fixed

$$I_{dn}(E, E_{max}) = \min_{\eta, V} \left(\frac{P - \lambda_{opt} V}{|\dot{E}|} \right)_{\dot{E}<0} \quad (19)$$

E fixed

The last step in minimizing J involves finding the optimum E_{max} for the specified range. A necessary condition for J to be minimum at some E_{max} is for the derivative of J with respect to E_{max} to vanish at E_{max} . This is done as follows. We compute the derivative of J for an increasing sequence of E_{max} , starting with $E_{max} = \max\{E_i, E_f\}$. As E_{max} is increased for fixed R , R_c decreases and two cases can occur:

- (1) $\delta J = 0$ for some E_{max} such that $0 < R_c \leq R$ or $\delta J = 0$ as $R_c \rightarrow 0$.
- (2) $\delta J < 0$ as $R_c > 0$.

We shall discuss case (1) in more detail than case (2) since case (1) applies to both aircraft models studied in the following sections of this paper.

Case (1)

For this case, the derivative of J with respect to E_{max} can be computed from Eq. (14) using Leibnitz's rule and Eqs. (12), (15), and (17) through (19):

$$\frac{dJ}{dE_{max}} = I_{up}^-(E_{max}, E_{max}) + I_{dn}^-(E_{max}, E_{max}) + R_c \left. \frac{d\lambda_{opt}}{dE} \right|_{E=E_{max}} \quad (20)$$

The quantities I_{up}^- and I_{dn}^- are limiting values of I_{up} and I_{dn} as $E \rightarrow E_{max}$ from below. In general, the limits must be evaluated for this case since both the numerators and denominators of the bracketed quantities in (18) and (19) can approach zero simultaneously as $E \rightarrow E_{max}$.

For the two types of aircraft studied in this paper, the functions I_{up}^- , I_{dn}^- , and λ_{opt} have special characteristics that have been observed in computations and can be verified analytically using polynomial representations for the aerodynamic and engine models given in the next section. First, the function $\lambda_{opt}(E_{max})$ has the general shape shown in Fig. 1. Second, the functions I_{up}^- , I_{dn}^- obey the relationship

$$I_{up}^-(E_{max}, E_{max}) + I_{dn}^-(E_{max}, E_{max}) = 0 \quad (21a)$$

Thus the values of the limit functions are equal in magnitude and opposite in sign. Moreover, at E_{max} the optimum controls satisfy the relationships:

$$\left. \begin{aligned} \pi_{opt} \\ V_{opt} \end{aligned} \right\} = \text{Arg. min}_{\pi, V} \left. \frac{P}{V} \right|_{\substack{E=E_{max} \\ E=0}} \\ = \text{Arg. min}_{\pi, V} \lim_{E \rightarrow E_{max}} \frac{P - \lambda_{opt} V}{\dot{E}} \Big|_{\dot{E} > 0} \\ = \text{Arg. min}_{\pi, V} \lim_{E \rightarrow E_{max}} \frac{P - \lambda_{opt} V}{\dot{E}} \Big|_{\dot{E} < 0} \quad (21b)$$

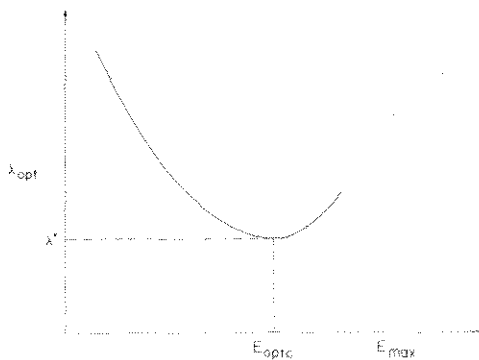


Fig. 1 Typical relationship between cruise efficiency and cruise energy, subsonic aircraft.

This relationship is illustrated by Fig. 2 in which is plotted the locus of optimum controls obtained from Eqs. (18) and (19) as a function of E . It is seen that the two branches of the locus converge to the controls obtained from Eq. (17) for cruise at E_{max} . Furthermore, it can be shown by analysis of the polynomial representation that the bracketed quantities in (18) and (19) have a local minimum at (π_c, V_c) with respect to admissible control variations. However, the continuity of the optimum controls at E_{max} depends on the aerodynamic characteristics and especially on the relationship between thrust and fuel flow. In particular, it is not generally true for the linear dependence often assumed in earlier work.^{3,4}

Substituting (21) into (20) yields the simplified form

$$\frac{dJ}{dE_{max}} \equiv R_c \left. \frac{d\lambda_{opt}}{dE} \right|_{E=E_{max}} = 0 \quad (22)$$

It follows immediately from Eq. (22) that a nonzero cruise distance can be optimum only if E_{max} yields the minimum of $\lambda_{opt}(E)$, which is designated as λ^* in Fig. 1. This result is consistent with the results of other workers, e.g., Schultz and Zagalsky.³ If the range is less than some minimum value, the maximum energy of the flight path will fall below the optimum cruise energy. In that case Eq. (22) requires zero cruise distance ($R_c = 0$). This fact simplifies computing the relationship between R and E_{max} . For each choice of E_{max} , one first computes $\lambda_{opt}(E_{max})$ and then R_{up} and R_{dn} using relations (15). In performing the range integrations, the optimum controls obtained from Eqs. (18) and (19) must be used. The range-energy relationship is then

$$\left. \begin{aligned} R(E_{max}) &= R_{up} + R_{dn}, & E_{max} < E_{optc} \\ R(E_{max}) &= R_{up} + R_{dn} + R_c, & E_{max} = E_{optc} \end{aligned} \right\} \quad (23)$$

By integrating (18) and (19) for each choice of E_{max} , the relationship between optimum cost and E_{max} can also be obtained:

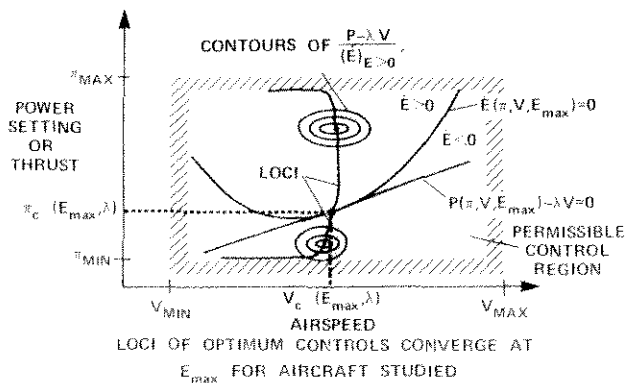


Fig. 2 Typical locus of optimum controls as a function of E .

$$J_{\text{opt}}(E_{\text{max}}) = \int_{E_L}^{E_{\text{max}}} I_{\text{up}}(E, E_{\text{max}}) dE + \int_{E_F}^{E_{\text{max}}} I_{\text{dn}}(E, E_{\text{max}}) dE + R(E_{\text{max}}) \lambda_{\text{opt}}(E_{\text{max}}) \quad (24)$$

Case (2)

In this case the quantity λ_{opt} loses its previous interpretation as a measure of cruise efficiency and instead becomes an adjoint variable λ , whose value must be chosen iteratively to achieve a specified range R . The condition which determines the maximum energy for a trial value of λ can be obtained by application of the maximum principle to Eqs. (14) and (15) with R_C set to zero.⁵ The condition is found to be

$$\min_{W, V} \left(\frac{P - \lambda V}{\dot{E}} \right)_{\dot{E} > 0}^{E = E_{\text{max}}} + \min_{W, V} \left(\frac{P - \lambda V}{|\dot{E}|} \right)_{\dot{E} < 0}^{E = E_{\text{max}}} = 0$$

For this case the optimum controls will generally not be continuous at the maximum energy point of the trajectory.

An essential requirement for implementing the algorithm on a computer is a routine for minimizing a function of two variables. Results presented in the next sections were obtained using an algorithm known, in the literature of nonlinear programming, as the method of local variations.⁶ This optimization algorithm does not require derivative calculations. The minimization over power setting can be eliminated *a priori* only for the minimum time performance index, $\alpha = 0$, since in that case the power setting is a bang-bang function of energy. Special provisions must also be made for computing I_{up} and

I_{dn} as E approaches E_{max} where the optimum controls yield values of \dot{E} near zero. A satisfactory approach is to decrease the integration step size as $E \rightarrow E_{\text{max}}$ and to stop when $|\dot{E}| < \dot{E}_{\text{min}}$. A value of 0.33 m/sec for \dot{E}_{min} was used in the results described in the following section.

Aerodynamic and Propulsion Models

The algorithm was used to study optimum trajectories for two types of aircraft: the CTOL aircraft, a 180-passenger tri-jet currently in short-haul service; and the STOL aircraft, a future-design, four-engine, 150-passenger, 700-m field length jet aircraft using augmentor flaps to achieve STOL performance, and a swept, supercritical airfoil to achieve a Mach 0.8 cruise speed. The design of the STOL was carried out in a recent NASA study.⁷

Aerodynamic forces for both types of aircraft are described by the following equations:

$$L = C_L S q \quad (\text{lift force}) \quad (25)$$

$$D = C_D S q \quad (\text{drag force}) \quad (26)$$

$$C_L = k_0 + k_1 \alpha \quad (\text{lift coefficient}) \quad (27)$$

where C_D is the drag coefficient, S the wing reference area, and q the dynamic pressure; $q = (1/2)\rho(h)V^2$. The air density ρ , as a function of altitude h , was obtained from the 1962 Standard Atmosphere. The drag coefficients for the two aircraft are parameterized as follows:

$$C_D = C_{D_0}(M) + K(M)(C_L - 0.1)^2 \quad (\text{CTOL aircraft}) \quad (28)$$

$$C_D = 0.019 + 0.0610 C_L^2 + \Delta(M, C_L) \quad (\text{STOL aircraft}) \quad (29)$$

where M is Mach number.

The constants in Eq. (27) and the Mach number corrections in (28) and (29) together with the masses and wing reference areas for the two aircraft are given in Tables 1 and 2.

Table 1 Aerodynamic data and weight for CTOL aircraft

M	0	0.70	0.76	0.80	0.82	0.84	0.85	0.86	0.87	0.88	0.89
$C_{D_0}(M)$	0.0173	0.0173	0.0174	0.0177	0.0179	0.0182	0.0186	0.0189	0.0195	0.0203	0.0218
$K(M)$	0.0864	0.0864	0.0932	0.103	0.113	0.128	0.141	0.169	0.184	0.211	0.241

Note: $k_0 = 0$, $k_1 = 0.1$, $S = 145 \text{ m}^2$, and $W = 68,200 \text{ kg}$.

Table 2 Aerodynamic data and mass for STOL aircraft

$C_L \backslash M$	0	0.62	0.64	0.66	0.68	0.70	0.72	0.74	0.76	0.77
Mach number and lift coefficient correction to drag coefficient, $\Delta(M, C_L)$										
0	0	0.0001	0.0002	0.0005	0.00075	0.0010	0.0013	0.0017	0.0026	0.0034
0.20	0	0.0001	0.0002	0.0005	0.00075	0.0010	0.0013	0.0017	0.0026	0.0034
0.25	0	0	0.0001	0.0002	0.0005	0.0009	0.0012	0.0016	0.0021	0.0026
0.30	0	0	0	0.0001	0.0003	0.0007	0.0010	0.0014	0.0020	0.0025
0.35	0	0	0	0.0001	0.0003	0.0007	0.0011	0.0014	0.0020	0.0024
0.40	0	0	0	0.0001	0.0003	0.0007	0.0011	0.0015	0.0021	0.0025

Note: $k_0 = -0.1$, $k_1 = 0.075$, $S = 255 \text{ m}^2$, and $W = 90,000 \text{ kg}$.

The aircraft propulsion systems are modeled using corrected engine parameters⁸ as follows:

$$\frac{T_P}{\delta} = f_T(\Pi/\sqrt{\theta}, M) \quad (30)$$

$$\frac{W_P}{\delta \sqrt{\theta}} = f_F(\Pi/\sqrt{\theta}, M) \quad (31)$$

where T_P and W_P are the thrust and fuel flow rate, respectively. The quantities δ and θ are pressure and temperature factors given by

$$\delta = \frac{p(h)}{p_0} \left(1 + \frac{\gamma-1}{2} M^2\right)^{\gamma/(\gamma-1)} \quad (32)$$

$$\theta = \frac{r(h)}{r_0} \left(1 + \frac{\gamma-1}{2} M^2\right) \quad (33)$$

where $r(h)/r_0$ and $p(h)/p_0$ are atmospheric temperature and atmospheric pressure ratios obtained from the 1962 Standard Atmosphere and $\gamma = 1.4$ is the air specific heat ratio. The quantity Π is the power setting, which for the CTOL aircraft is actual rotor revolution per minute and for the STOL aircraft is defined as

$$\Pi = \Pi_{In}/\theta \quad (34)$$

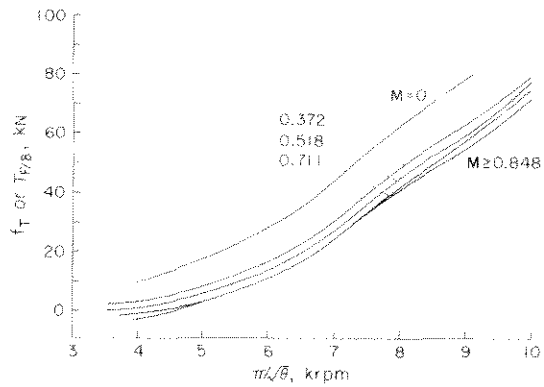
where Π_{In} is the actual turbine inlet temperature. The corrected thrust and fuel flow curves per engine for the CTOL and STOL aircraft are given in figures 3 and 4, respectively. (In Fig. 4, and in subsequent discussions of STOL trajectories, Π is referred to as T_c , the corrected turbine inlet temperature.)

Fixed-Range Optimum Flight Paths: CTOL Aircraft

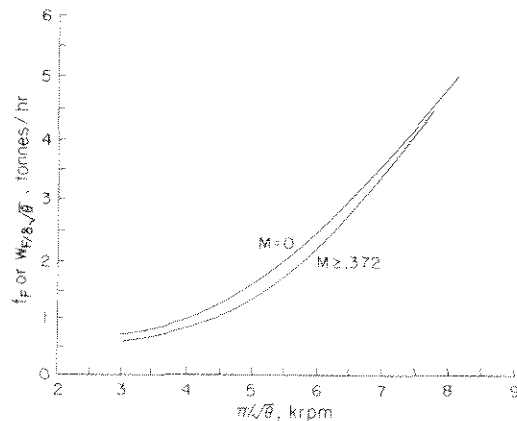
The first step in the implementation of the algorithm is the computation of cruise efficiency as a function of maximum energy (Eq. (17)) for different values of σ . The results of this computation for a fixed mass of 68,200 kg are plotted in Fig. 5 in cruise-fuel-efficiency (kg/km) and cruise-air-speed (m/sec) coordinates. The solid heavy line gives the envelope of optimum cruise conditions as σ ranges from zero to 1. Points A and B define the fuel efficiencies and airspeeds for minimum fuel and minimum time, respectively. Minimum-fuel cruise occurs at an altitude of 10 km, which is about 1 km below the ceiling, whereas minimum-time cruise (maximum airspeed) occurs at an altitude of 5.5 km. Figure 5 also shows the loci of fuel efficiency and airspeed for $\sigma = 0.5$ as the maximum energy is allowed to vary over its possible range. It was shown earlier that no cruise can take place in the optimum trajectories except at the absolute optimum cruise represented by points on the solid line. Point C on the $\sigma = 0.5$ cruise locus achieves this optimum value denoted by λ^* . Any other point on the $\sigma = 0.5$ cruise locus corresponds to a λ_{opt} value greater than λ^* and therefore corresponds to a range less than the smallest range containing a nonzero cruise distance.

In computing the cruise efficiency, the actual rotor revolutions per minute were restricted to maximum cruise power setting of the engine which is modeled as:

$$\Pi_{MAX.} = \begin{cases} 7.40 + 0.18(h/3 - 1.5), & h \leq 7.65 \text{ km} \\ 7.66 & \text{otherwise} \end{cases}$$

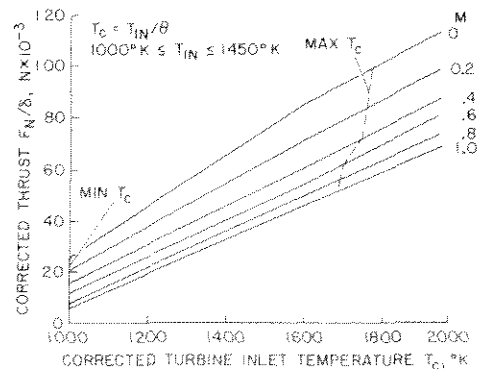


(a) Corrected thrust as a function of Mach number and corrected power setting.



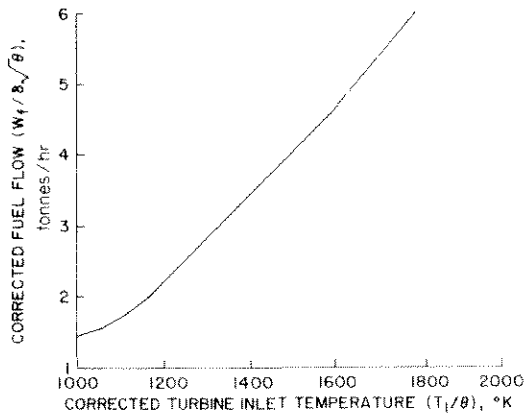
(b) Corrected fuel flow rate as a function of Mach number and corrected power setting.

Fig. 3 CTOL aircraft: thrust and fuel flow rate corrections.



(a) Corrected thrust as a function of corrected turbine inlet temperature.

Fig. 4 STOL aircraft: thrust and fuel flow rate corrections.



(b) Corrected fuel flow rate as a function of corrected turbine inlet temperature.

Fig. 4 STOL aircraft: thrust and fuel flow rate corrections - Concluded.

In computing the optimum climb and descent strategies, dynamic pressure q is limited to 35 N/m^2 , the altitude is constrained to be larger than zero, and the actual engine power setting is bounded from below by 3.95 k rpm. For $0.2 < \sigma \leq 1$, the power setting is limited to maximum climb which is modeled as

$$\Pi_{\text{climb}} = \begin{cases} 7.70 + 0.027h, & h \geq 7.62 \text{ km} \\ 7.90, & \text{otherwise} \end{cases} \quad (36)$$

For $0 \leq \sigma \leq 0.2$, which corresponds to near minimum-time missions, the power setting is limited to maximum cruise during the entire flight profile. This limitation will exclude prolonged operation of the engine at maximum allowable power setting which, from the point of view of cost of maintenance, might be undesirable.

The climb and descent range, time, and fuel are calculated by integrating Eqs. (15) and the following two equations using the trapezoidal rule:

$$T_{\text{up}} = \int_{E_i}^{E_{\text{max}}} \left(\frac{1}{\dot{E}} \right)_{\dot{E}>0} dE, \quad T_{\text{dn}} = \int_{E_f}^{E_{\text{max}}} \left(\frac{1}{|\dot{E}|} \right)_{\dot{E}<0} dE \quad (37)$$

$$F_{\text{up}} = \int_{E_i}^{E_{\text{max}}} \left(\frac{W_F}{\dot{E}} \right)_{\dot{E}>0} dE, \quad F_{\text{dn}} = \int_{E_f}^{E_{\text{max}}} \left(\frac{W_F}{|\dot{E}|} \right)_{\dot{E}<0} dE \quad (38)$$

It was shown earlier that as $E \rightarrow E_{\text{max}}$, the optimum power setting and optimum velocity approach the cruise values corresponding to $\lambda_{\text{opt}}(E_{\text{max}})$; i.e., \dot{E} approaches zero causing the integrands of Eqs. (15), (37), and (38) to diverge. To circumvent this problem, a decreasing step size for ΔE is employed as $E \rightarrow E_{\text{max}}$. The criterion used for obtaining an appropriate integration step size is given by

$$\Delta t = \frac{\Delta E}{|\dot{E}|} < 30 \text{ sec} \quad (39)$$

where Δt is the time increment. The integration process is stopped when $|\dot{E}| \leq 0.3 \text{ m/sec}$. The sensitivity of the minimum-fuel trajectories with

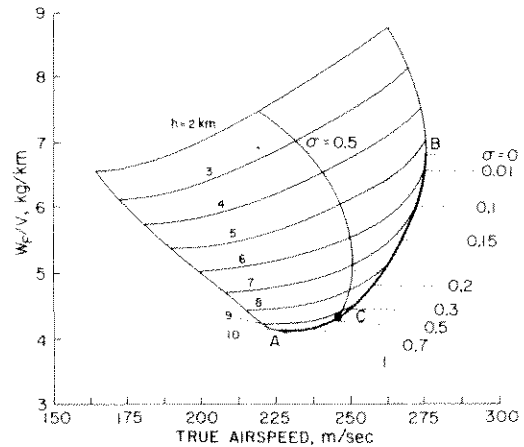


Fig. 5 Cruise operating cost efficiency, CTOL aircraft.

respect to Δt was studied. If Δt is restricted to be less than 15 sec, rather than 30 sec, then the total time and fuel of the mission for a fixed range are changed by only 0.3 percent.

Figure 6 shows optimum climb and descent trajectories in altitude-velocity coordinates for minimum fuel ($\sigma = 1$), minimum time ($\sigma = 0$), and an intermediate value of $\sigma = 0.5$. For each of the three values of σ , optimum trajectories corresponding to different total ranges are plotted, with the range indicated on each trajectory. For each value of σ , the trajectory with the largest value of E_{max} is the optimum trajectory corresponding to the smallest range with a nonzero cruise segment. The only possible cruise points are also shown in figure 6. Note that the velocity altitude profile at E_{max} is continuous for each optimum trajectory.

Figure 7 plots altitude versus range of several optimum trajectories, each for a different σ value. All trajectories cover a range of 800 km. As σ approaches zero, the optimum cruise altitude decreases while the range covered in the climb trajectory increases.

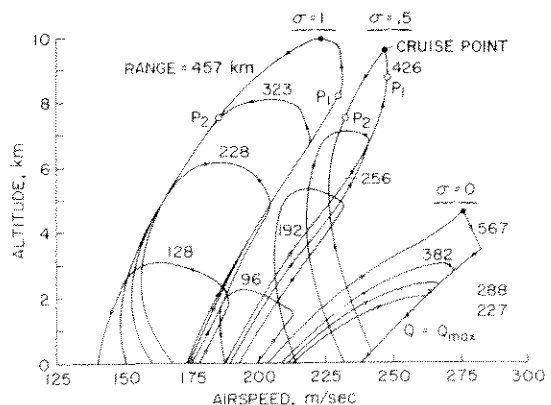


Fig. 6 Speed-altitude profiles, CTOL aircraft.

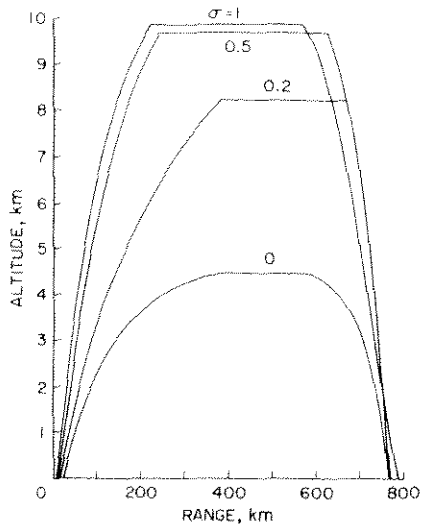


Fig. 7 Altitude-range profiles, CTOL aircraft.

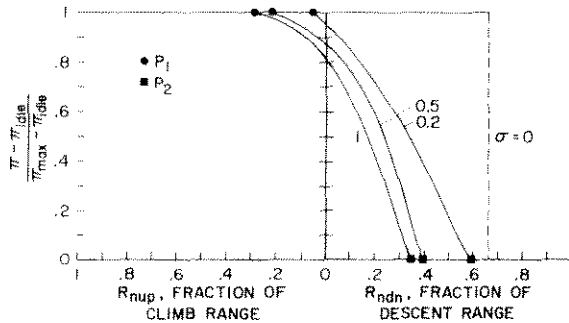


Fig. 8 Percent throttle setting versus percent climb or descent range covered with an 800-km fixed range, CTOL aircraft.

Normalized throttle variations versus normalized range are plotted in figure 8 where Π is the actual rotor revolutions in krpm; $\Pi_{idle} = 3.95$ krpm is the idle throttle setting; Π_{max} is maximum climb throttle setting for $0.2 \leq \sigma \leq 1$ and is the maximum cruise throttle setting for $0 < \sigma \leq 0.2$; R_{nup} is the distance from the maximum energy point divided by R_{up} and R_{dn} is the equivalent fraction of R_{dn} . The intersection of these curves with the throttle setting axis corresponds to the cruise throttle setting. It is seen that as $\sigma \rightarrow 0$ the fraction of the climb range covered at maximum throttle setting increases and the fraction of descent range covered at idle throttle setting decreases. This is expected as time is weighed more and fuel less in the performance index. The portion of the optimum trajectories corresponding to intermediate values of throttle setting lies between points P_1 and P_2 . The same notation is used to indicate the corresponding points on two of the trajectories in figure 6.

Simulation of Minimum Fuel Profiles

The minimum fuel trajectories consist of acceleration at level flight to a speed which is nearly independent of the range, climb at maximum power setting, a segment during which the power setting is reduced from maximum to idle, and a descent at

idle (see figs. 6 through 8). In addition, if the range to be covered is larger than 457 km, a cruise segment at $V_c = 226$ m/sec and $H_c = 10$ km will be present.

It has been found that irrespective of a given range, the minimum-fuel flight profiles can be replaced by approximating trajectories that consist of only two segments: (1) a climb at maximum climb power setting and 152.5 m/sec equivalent airspeed (EAS) and (2) a descent portion at idle and 128 m/sec (EAS). The change from the climb to the descent portion is made at an energy level which gives the desired range. The total fuel consumption associated with the approximating trajectories is about 1.5 percent higher than that of the minimum-fuel flight profiles.

Minimum Time Profiles

Minimum time trajectories, which correspond to $\sigma = 0$, are shown in figures 6, 7, and 8 along with trajectories for the other σ values. For this case, figure 8 shows that power is either at idle or at maximum. The switch from maximum to idle occurs in the decreasing energy regimen when the airspeed has decreased to $V_{E_{max}}$, the airspeed at the maximum energy point. During a part of the descent the airspeed follows the design dive flight placard of an EAS of 238 m/sec.

The structure of minimum time flight profiles can also be derived from the observation that the function to be minimized at each energy level is $[1 - (V/V_{E_{max}})]/|V(T-D)|$ where $V_{E_{max}} = 1/\lambda$ is the velocity associated with the maximum energy of the particular trajectory. During descent, if $V < V_{E_{max}}$, the minimizing value of the power setting is at idle; on the other hand, if $V > V_{E_{max}}$, the minimizing value is the maximum power setting.

Minimum DOC Profiles

By letting distance be a parameter, a spectrum of optimum trajectories from minimum time to minimum fuel may be obtained as σ is varied from zero to 1. The time-fuel tradeoff generated by this spectrum is plotted in figure 9 for several distances. It is characteristic that these tradeoff curves approach a horizontal slope near $\sigma = 1$ and a vertical slope near $\sigma = 0$. Given the relative dollar costs of time and fuel one can use Eq. (5) to calculate the value of $0 < \sigma < 1$ which will minimize the DOC. In addition, if the range is also specified, then the time and the fuel can be read from figure 9. As an example, assume 13.2 cents/kg fuel cost and \$300/hr time cost, typical costs for the operation of this particular aircraft. Then the corresponding value of σ will be 2/3. This σ value falls roughly on the knee of the constant range tradeoff curve of figure 9.

Fixed-Range Optimum Flight Paths: STOL Aircraft

Except for minor variations the same methods were used for the STOL aircraft as for the CTOL. Because the STOL model used is the result of a preliminary design study, it is important to note that the actual numerical values presented might be subject to considerable revision in the future. Nevertheless, the results serve to illustrate the effects which are peculiar to an aircraft equipped for the use of powered lift.

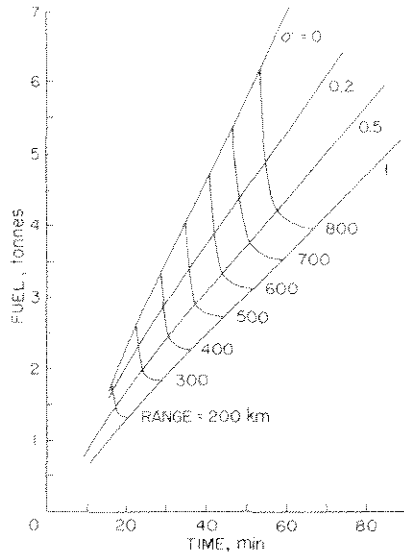


Fig. 9 Time-fuel tradeoff for fixed ranges, CTOL aircraft.

The method of keeping the thrust setting within the allowable limits differed somewhat from the case of the CTOL aircraft. The turbine inlet temperature T_{in} was limited in the optimization to $1000^{\circ}\text{K} < T_{in} < 1450^{\circ}\text{K}$ and the corrected turbine temperature, $T_c = T_{in}/\theta$, was limited as shown by the "max T_c " boundary in figure 4(a). Regardless of which constraint is governing, the lower limit will be referred to as "flight-idle" and the upper limit as "maximum thrust."

The optimization for this aircraft over most of the descent portion (except when $\sigma = 0$) was complicated by the existence of two local minima in the integrand of Eq. (19). These local minima varied, from being widely separated to nearly coincident, depending on the energy level. The function minimization routine located both local minima, and then chose the controls corresponding to the smallest of the two as the optimum controls.

Figure 10 shows the contours of cruise fuel efficiency versus true airspeed for different values of altitude using an aircraft weight of 90,700 kg. The minimum fuel cruise condition occurs at an altitude of 11 km and a speed of 200 m/sec. As in the case of the CTOL aircraft, this point is below the ceiling; however, the difference is only about 100 m in this case. The minimum-time cruise condition occurs near an altitude of 6 km and an airspeed of 230 m/sec. A tradeoff between time and fuel can be obtained by selecting different operating points along any of the altitude contours. At all altitudes, the curves are quite flat near the minimum fuel point, and a speed change of about 7 percent is required to produce a 1-percent change in fuel. The fuel consumption near the minimum time curve increases more rapidly with speed, and an increase of 5 percent in time produces about an 8 percent reduction in fuel, except at the highest altitudes. Also, along the minimum-time curve the fuel consumption increases rapidly with decreasing altitude while corresponding changes in speed are small.

A series of minimum-fuel and minimum-time trajectories was calculated for various values of E_{max} up to and including the minimum-fuel and

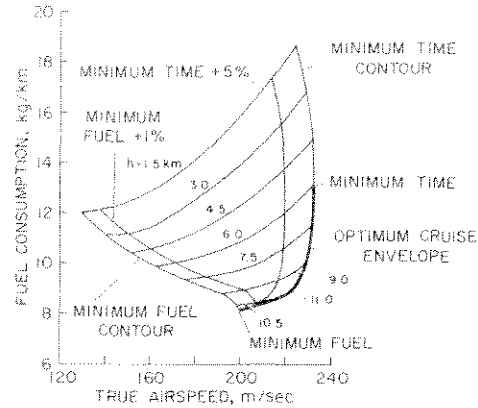


Fig. 10 Cruise fuel efficiency, STOL aircraft.

minimum-time cruise energies. The initial and final energies were 1.5 km in all cases, and a lower altitude limit of 150 m was imposed. The results for intermediate values of σ were not determined for this aircraft.

Minimum Fuel Profiles

Figure 11 gives the altitude-range profiles for three minimum-fuel trajectories having no cruise section. The maximum energy for the longest trajectory is the minimum-fuel cruise energy. Note that all of the trajectories follow the same ascent path until maximum energy is reached. The flight-path angle appears to be discontinuous between ascent and descent at the scale used in the figure, but the use of sufficiently small increments in energy shows that this is not the case. For short ranges, most of the distance is covered during the descent portion, but as the range, and hence the maximum energy increases, a greater portion of the distance is covered during ascent. This is because the energy rate and the corresponding flight-path angle approach zero slowly near the minimum-fuel cruise energy. The final portion of each trajectory consists of a steep descent followed by a short section of level flight at the low altitude limit.

The speed-altitude profiles in figure 12 are for the minimum-fuel trajectories just discussed and two minimum-time trajectories. In the minimum-fuel case, the ascent and higher altitude portion of the descent segments are quite similar to the results presented earlier for the CTOL aircraft. In this region maximum thrust is used for climb, and flight-idle is used for descent, except near the maximum energy, where a gradual transition is made to or from the cruise thrust. In the lower portion of the descent, the airspeeds become very high and thrust settings greater than flight-idle are used to help attain the high speed, after which the thrust is again reduced.

As the aircraft approaches the maximum speed on the descent trajectory (fig. 12), the magnitude of the flight-path angle and the magnitude of the acceleration become very large. For example, consider the case of the trajectory for the longest range (764 km). A 500-m reduction in energy between points A and B occurs in 24 sec and is accompanied by a speed increase of 43 m/sec and an altitude change of nearly 1.6 km. During this interval the flight-path angle reaches -37° . Although the diving segments become shallower at lower values of E_{max} ,

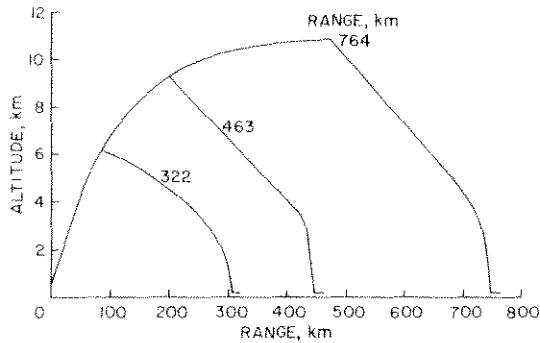


Fig. 11 Altitude-range profiles, STOL aircraft.

the trajectories appear to approach the constant energy transitions encountered in other studies.²

The steeply diving portions are probably caused by the high values of flight-idle thrust, and hence fuel flow to the engines providing powered lift for this STOL aircraft. At low altitudes, where the fuel consumption is high, fuel usage is minimized by descending at high speed and then decelerating to the final energy as rapidly as possible.

The high speeds at low altitudes and the large decelerations and flight-path angles encountered in the descent are unacceptable for passenger aircraft. One possible constraint, which provides an acceptable suboptimum trajectory for approximating the minimum-fuel case, is illustrated by the dashed lines in figure 12. For ascent, the indicated airspeed was restricted to a maximum of 130 m/sec (250 knots) and for descent the limit was chosen to fit the envelope of the upper portions of the descent segments. This limit provides fairly smooth transitions between the constrained and unconstrained portions.

Minimum Time Profiles

The minimum-time profiles in figure 12 are similar to those shown for the CTOL aircraft. The longest range trajectory (1064 km) just reaches the minimum time-cruise energy. The horizontal portions result from constraining the altitude to be at least 150 m; the initial and final energy levels were 1.5 km. Maximum thrust is required almost during the entire trajectory, except during the final horizontal segment for $V < V_C$ when it must be at flight-idle. The maximum speed during descent is limited by the drag increase with Mach number rather than by a control constraint. The magnitude of the flight-path angle never exceeds 4° .

Fuel and Time Tradeoff of Trajectories

The fuel and time used for various ranges for the minimum-time, minimum-fuel, and constrained-trajectories are plotted in figure 13, with the ranges indicated on the curves. The curves for intermediate σ values were not obtained for the STOL aircraft. The effects of constraining airspeed in the minimum-fuel case are shown by the dashed line in figure 13. The constraint increases the cost in both fuel and time at each range. The increased costs occur almost entirely during descent and are attributed to the elimination of the high

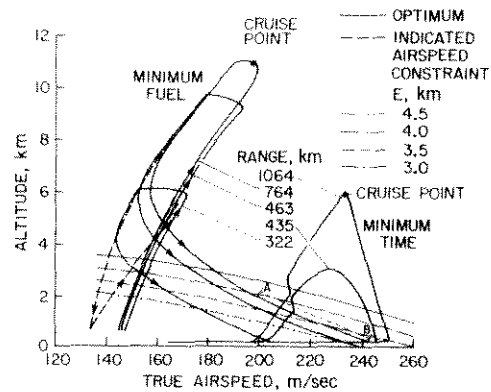


Fig. 12 Speed-altitude profiles, STOL aircraft.

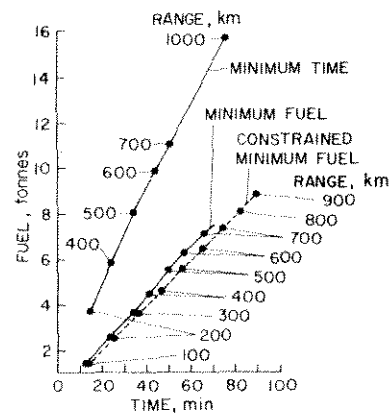


Fig. 13 Fuel and time requirements for fixed ranges, STOL aircraft.

speed segment during descent. A less severe speed constraint for descent (e.g., the one used for ascent) would provide a cost nearer the optimum if a satisfactory transition could be made to the optimum.

Since the ascent portions of the optimum and constrained trajectories are almost identical, it is desirable to compare costs only during the descent portion. The lower airspeeds in the constrained trajectory resulted in lower magnitudes of flight-path angle and energy rate, which in turn produced a larger range and longer flight time for descent from a given maximum energy. For the case of the maximum energy equal to the optimum cruise energy, the ranges were equalized to 891 km by adding an appropriate cruise section to the optimum trajectory. In this case, the constrained descent required about 10 percent more fuel and 19 percent more time than the minimum-fuel cruise and descent covering the same range.

Conclusions

By using the aircraft's total energy (kinetic plus potential) as the independent variable in the climb and descent segments, an efficient algorithm has been developed for computing fixed-range optimum trajectories for short-haul aircraft. The good computational efficiency of the algorithm makes it attractive for parametric studies as well as for possible on-board implementation. In this paper, fuel cost and flight range were selected as parameters and used to compute optimum time-fuel tradeoff

curves for the in-service CTOL aircraft. Such curves can help an airline in determining the best operating strategy in periods of fluctuating fuel prices. The optimum trajectories for both the CTOL and STOL aircraft are characterized by the absence of a cruise segment unless the range of the mission exceeds a minimum value. For the CTOL aircraft, the optimum controls, consisting of airspeed and engine power setting, were smooth functions of the energy, thereby yielding flyable, though nonstandard, trajectories. However, additional work is required to define the on-board displays, computers, and auto-pilot navigation system interfaces required for the pilot to be able to fly the optimum trajectories. For the STOL aircraft, the airspeed was nearly discontinuous with respect to energy at one energy level during the minimum fuel descent. Under the worst conditions, elimination of the steep dive, required to fly such a descent, increased fuel consumption by 10 percent and the time to fly by 19 percent compared to the optimum descent trajectory.

References

- ¹Anon., "Standard Method of Estimating Comparative Direct Operating Costs of Turbine Powered Airplanes," Air Transport Association of America, Washington, D.C., Dec. 1967.
- ²Bryson, A. E., Jr., Desai, M. N., and Hoffman, W. C., "Energy State Approximation in Performance Optimization of Supersonic Aircraft," *Journal of Aircraft*, Vol. 6, No. 6, Nov.-Dec. 1969, pp. 481-488.
- ³Schultz, R. L. and Zagalsky, N. R., "Aircraft Performance Optimization," *Journal of Aircraft*, Vol. 9, No. 2, Feb. 1972, pp. 108-114.
- ⁴Zagalsky, N. R., "Aircraft Energy Management," AIAA Paper 73-228, 1973.
- ⁵Pontryagin, L. S. et al., *The Mathematical Theory of Optimal Processes*, transl. by K. N. Trirogoff, Interscience, New York, 1962.
- ⁶Polak, E., *Computational Methods in Optimization: A Unified Approach*, Academic Press, New York, 1971.
- ⁷Anon., "Study of Quiet Turbofan STOL Aircraft for Short-Haul Transportation," Final Rept., Vol. II, CR-114,607, June 1973, NASA.
- ⁸Hesse, W. J. and Mumford, N. V. S., Jr., *Jet Propulsion for Aerospace Applications*, Pitman Publishing Corp., New York, 1964, pp. 275-283.